Available online at www.sciencedirect.com
SCIENCE DIRECT®
Journal of Structural Biology 149 (2005) 7–16
Journal of Structural Biology
www.elsevier.com/locate/yjsbi

Structural and orientational constraints of bacteriorhodopsin in purple membranes determined by oriented-sample solid-state NMR spectroscopy

Miya Kamihira[a,1], Thomas Vosegaard[b,1], A. James Mason[a,2], Suzana K. Straus[a,3], Niels Chr. Nielsen[b,*], Anthony Watts[a,*]

[a] *Biomembrane Structure Unit, Department of Biochemistry, Oxford University, South Parks Road, Oxford OX1 3QU, United Kingdom*
[b] *Laboratory for Biomolecular NMR Spectroscopy, Interdisciplinary Nanoscience Center (iNANO) and Department of Chemistry, University of Aarhus, DK-8000 Aarhus C, Denmark*

Received 28 May 2004, and in revised form 23 September 2004

Abstract

We report for the first time, oriented-sample solid-state NMR experiments, specifically polarization inversion spin exchange at the magic angle (PISEMA) and ^{1}H–^{15}N heteronuclear chemical shift correlation (HETCOR), applied to an integral seven-transmembrane protein, bacteriorhodopsin (bR), in natural membranes. The spectra of [^{15}N]Met-bR revealed clearly distinguishable signals from the helical and loop regions. By deconvolution of the helix resonances, it was possible to establish constraints for some helix tilt angles. It was estimated that the extracellular section of helix B has a tilt of less than 5° from the membrane normal, while the tilt of helix A was estimated to be 18–22°, both of which are in agreement with most crystal structures. Comparison of the experimental PISEMA spectrum with simulated spectra based on crystal structures showed that PISEMA and HETCOR experiments are extremely sensitive to the polytopic protein structure, and the solid-state NMR spectra for membrane-embedded bR matched most favorably with the recent 1FBB electron crystallography structure. These results suggest that this approach has the potential to yield structural and orientational constraints for large integral polytopic proteins whilst intercalated and functionally competent in a natural membrane.

Keywords: Solid-state NMR spectroscopy; PISEMA and HETCOR; Bacteriorhodopsin; Oriented purple membrane; Simulation

1. Introduction

Bacteriorhodopsin (bR) is the light-driven proton pump of *Haloarchaea*. It is a 26 kDa membrane protein comprising seven transmembrane α-helices and a chromophore retinal covalently linked to Lys-216, and could be the structural paradigm of G-protein-coupled receptors and other proteins (Lanyi, 1993, 1997; Mathies et al., 1991; Ovchinnikov, 1982; Stoeckenius and Bogomolni, 1982). It forms a two-dimensional hexagonal crystalline lattice arranged in trimeric units in the native purple membrane (PM). In the PM, bR orients well on glass plates (Fitter et al., 1999; Papadopoulos et al., 1990; Seiff et al., 1985), which preserves the directional quality of the protein and maintains structural and functional integrity under a wide range of conditions, such as pH, temperature, humidity, and chemical environment (Oesterhelt et al., 1991).

* Corresponding authors. Fax: +44 1865 275234 (A. Watts), +45 86196199 (N.Chr. Nielsen).
E-mail addresses: ncn@chem.au.dk (N.Chr. Nielsen), anthony.watts@bioch.ox.ac.uk (A. Watts).
[1] These authors contributed equally to this work.
[2] Present address: Institut für Biophysikalische Chemie, J.W. Göethe-Universität Frankfurt, Marie-Curie-Str. 9, 60439 Frankfurt, Germany.
[3] Present address: Department of Chemistry, University of British Columbia, 2036 Main Mall, D405, Vancouver, BC, Canada V6T 1Z1.

1047-8477/$ - see front matter © 2004 Elsevier Inc. All rights reserved.
doi:10.1016/j.jsb.2004.10.002

Recently, a number of X-ray diffraction (XRD) structures of crystalline bR have been determined (Hirai and Subramaniam, 2003) to a resolution of up to 1.43 Å for the ground state, and a number of functional photo-intermediates (Edman et al., 1999; Faham and Bowie, 2002; Lanyi and Schobert, 2002; Luecke et al., 1999a,b; Royant et al., 2001; Sass et al., 2000; Schobert et al., 2002). In all cases, some of the loops have not been well resolved, and the boundary regions between helices and loops sometimes are indistinct or differently defined in different crystal structures. Solid-state NMR spectroscopy has provided complementary structural information. For example, the orientational changes in the retinal during the photocycle (Ulrich et al., 1992, 1994, 1995) and some residues involved in the active site, such as Lys and Arg (Herzfeld and Lansing, 2002), have been determined, and dynamic information has been determined for helices, loops, and the C-terminus of bR in the PM (Saitô et al., 1998, 2000, 2002).

A powerful solid-state NMR method for the determination of protein structure and conformation is the so-called polarization inversion spin exchange at the magic angle (PISEMA) experiment (Ramamoorthy et al., 1999; Wu et al., 1994), which correlates the orientation-dependent, anisotropic ^{1}H–^{15}N dipole–dipole couplings and ^{15}N chemical shift interactions. For oriented samples, this experiment has provided high-resolution orientational constraints on peptide planes for protein fragments and single-transmembrane peptides embedded in phospholipid bilayers (Kim et al., 1998; Marassi et al., 1999, 2000; Nishimura et al., 2002; Song et al., 2000). For α-helix or β-sheet structures in uniformly ^{15}N-labeled peptides (~30–40 residues), the PISEMA experiment leads to wheel-like patterns called "polarization index slant angle (PISA) wheels" (Marassi and Opella, 2000; Wang et al., 2000). From such wheels it is possible to determine the secondary structure, the tilt angles of α-helices or β-sheets, and in favorable cases sequential assignment of all resonances on the basis of a single unique resonance assignment (Denny et al., 2001; Marassi, 2001). The application of the method to a larger (190-mer) membrane protein (colicin) has also been demonstrated, with confirmation of partial penetration into the membrane of some residues (Kim et al., 1998).

Another fundamental ingredient in solid-state NMR of membrane proteins is the ability to simulate experimental spectra numerically to extract precise structural parameters from experimental spectra, and evaluate the compatibility with structures determined by direct means. These needs are served by the simulation program for solid-state NMR spectroscopy (SIMPSON, open-source software, download site: http://www.bionmr.chem.au.dk) (Bak et al., 2000) which operates essentially as a computer spectrometer. In combination with another program, SIMMOL (open-source software, download site: http://www.bionmr.chem.au.dk), that reads in atomic coordinates in the protein data bank (PDB) format, and generates typical or user-defined NMR parameters (Bak et al., 2002), it is possible to simulate expected NMR spectra from high-resolution crystal structures.

Here, oriented solid-state NMR methods were used in conjunction with SIMPSON/SIMMOL to obtain structural information on bR in native PM. Specifically, we recorded and analyzed PISEMA and ^{1}H–^{15}N heteronuclear correlation (HETCOR) spectra for [^{15}N]Met-bR, demonstrating for the first time the application of this methodology to large polytopic integral proteins. Parallel use of these two methods may give the potential to determine structures of membrane proteins, because PISEMA provides good signal separation for *transmembrane helices* with modest tilt angles relative to the bilayer normal, while HETCOR provides good signal separations for tilt angles in the 60–90° regime being typical for *in-plane structures* or *loop regions* (Marassi, 2001; Vosegaard and Nielsen, 2002). Since the labeled residues chosen here are sparsely located not in a single helix but in helices, A, B, D, E, and G, and in loops in bR, the PISEMA and HETCOR spectra are not easy to assign nor show such a good separation of signals as those reported for single-transmembrane peptides. In addition, mosaic spread, molecular disorder, and inherent dynamics cause spectral line-broadening which need to be taken into account (Straus et al., 2003). However, the spectra allow clear distinction of helix- and loop-located resonances, and using SIMPSON and SIMMOL they can be deconvoluted to provide information about helix tilt angles and structural constraints which can be compared with crystal structures. This is a first step towards oriented solid-state NMR characterization of large integral membrane proteins in natural membranes.

2. Materials and methods

2.1. Sample preparation

[^{15}N]Met-bR was prepared by growing *Halobacterium salinarium* strain L33 using a synthetic medium (Helgerson et al., 1992) containing L-methionine (^{15}N, 98%) from Cambridge Isotope Laboratories (Andover, MA, USA). PM isolated and purified by the procedure of Oesterhelt and Stoeckenius (1974) was oriented on the surface of 30 thin glass plates ($8 \times 10 \times 0.06$–0.08 mm) (Paul Marienfeld GmbH KG, Lauda-Königshofen, Germany) by slowly evaporating 3 mg/ml (115 μM) of PM suspension in deionized water. In this way, uniaxial films with good orientation of the purple membrane patches parallel to the plates are formed as determined by neutron scattering (Papadopoulos et al., 1990; Seiff et al., 1985). After air-drying, the glass plates

containing a total of about 20 mg of [^{15}N]Met-bR (0.77 μmol) were stacked and sealed in Parafilm in a polyethylene tube (RS Components, Northants, UK).

2.2. Solid-state NMR spectroscopy

NMR spectra were recorded on a Varian CMX infinity 400 (1D ^{15}N CP) or Varian Unity-INOVA 400 (PISEMA and HETCOR) spectrometer equipped with home-built ^{15}N/^{1}H double-tuned flat-coil probe with a 4-turn coil of inner dimensions $11 \times 12 \times 4$ mm accommodating a stack of glass plates oriented perpendicular to the external magnetic field (B_0). The 1D experiment used a ^{1}H 90° pulse length of 5 μs and CW decoupling (40 kHz). The PISEMA experiment used a ^{1}H 90° pulse length of 4 μs and cross-polarization with mismatch-optimized IS transfer (CP-MOIST) (Levitt, 1991) for a duration of 1 ms with radiofrequency (rf) field strengths of ~40 kHz on the two channels. The ^{15}N and ^{1}H rf field strengths were 42.7 and 34.9 kHz, respectively, during the spin-exchange at the magic angle (SEMA) block (Bielecki et al., 1990; Lee and Goldburg, 1965), while a ^{1}H rf field strength of 65 kHz was used for CW decoupling. 8600 transients with a relaxation delay of 1.5 s were recorded for each of the 32 t_1 increments. The HETCOR experiment used a ^{1}H 90° pulse length of 4 μs followed by t_1 evolution under frequency-switched Lee–Goldburg (FSLG) (Bielecki et al., 1990) homonuclear decoupling with a ^{1}H rf field strength of 44.8 kHz and t_1 incremented in steps of three FSLG blocks. Following the t_1 evolution, the x or y component of the ^{1}H coherence was stored along z to obtain hypercomplex data, and transferred to ^{15}N by a SEMA period of 100 μs to ensure selective ^{1}H^{N} to ^{15}N transfer. The ^{15}N and ^{1}H ppm scales were referenced to liquid ammonia by an external $^{15}NH_4Cl$ powder sample at 39.8 ppm and to TMS by external water solutions, respectively. For all experiments the ^{1}H and ^{15}N transmitters were placed at 10 and 130 ppm, respectively. All NMR spectra were recorded at −20 °C to reduce effect of sample heating and improve CP efficiency. The indirect axis of the PISEMA and HETCOR spectra was compensated by theoretical scaling factors of $\sqrt{2/3}$ and $\sqrt{1/3}$, respectively.

2.3. Computational details

All numerical simulations were performed using the open-source SIMPSON (Bak et al., 2000) and SIMMOL (Bak et al., 2002) programs allowing PISEMA and HETCOR spectra to be calculated using typical secondary structural elements or atomic coordinates from other sources (Bak et al., 2002; Bjerring et al., 2003; Vosegaard and Nielsen, 2002; Vosegaard et al., 2002). The simulations assumed the following secondary-structure independent parameters: ^{15}N chemical shift: $\delta_{xx} = 61$ ppm, $\delta_{yy} = 80$ ppm, $\delta_{zz} = 228$ ppm, $\Omega_{PE} = \{-90°, -90°, -17°\}$; ^{1}H shift: $\delta_{xx} = 3$ ppm, $\delta_{yy} = 8$ ppm, $\delta_{zz} = 17$ ppm, $\Omega_{PE} = \{90°, -90°, 90°\}$; ^{1}H–^{15}N dipolar coupling: 9940 Hz (see Bak et al., 2002 for details). The magnitudes of the ^{15}N chemical shift tensors were estimated from magic angle oriented sample spinning (MAOSS) experiments on [^{15}N]Met-bR (Mason et al., 2004). On the basis of numerically simulated spectra using high-resolution XRD coordinates (1C3W) (Luecke et al., 1999b), we investigated various NMR methods and isotope labeling strategies. A good compromise between information content and resolution was found for [^{15}N]Met-bR in PM using a combination of PISEMA and HETCOR experiments.

Two approaches are pursued for the analysis of the experimental spectra: (i) a "blind" approach where no knowledge of the bR structure is employed and (ii) investigation of possible conformations of known bR structures being compatible with the experimental PISEMA spectrum. For the first approach, the helix region of the experimental spectrum was deconvoluted by fitting it to seven resonances corresponding to Met-20, 32, 56, 60, 118, 145, and 209. Since the resolution of this region is not sufficient to resolve seven discrete resonances, we performed 1000 individual optimizations using seven sets of ^{1}H–^{15}N dipolar couplings, ^{15}N chemical shifts, and Gaussian line-widths, with random starting values in the range of 8500 ± 1200 Hz, 200 ± 30 ppm, and 800 (^{1}H–^{15}N) and 500 Hz (^{15}N), respectively. This enabled discrimination of the seven resonances in certain domains of the spectra, each of which may be approximated by an elliptical shape. Using ^{15}N chemical shifts and ^{1}H–^{15}N dipolar couplings corresponding to the ellipses, restrictions of the helices (tilt angles (τ) with respect to B_0 and rotational pitch (ρ) angles) were calculated assuming that the residues belong to ideal α-helices ($\phi = -65°, \psi = -40°$).

For the second approach, the PISEMA spectra were calculated on basis of different bR crystal structures. Specifically, we present results from PDB access codes of 1C3W (Luecke et al., 1999b), 1KME (Faham and Bowie, 2002), and 1FBB (Subramaniam and Henderson, 2000). 1C3W was determined with 1.55 Å resolution by XRD using a 3D crystal grown from lipidic cubic phase (Luecke et al., 1999b). 1KME, determined by XRD at 2.0 Å resolution, was obtained from a 3D crystal grown from unique bicelles (Faham and Bowie, 2002). 1FBB is a recent 2D crystal structure at 3.2 Å resolution determined by electron diffraction (Subramaniam and Henderson, 2000). For 1KME, aligned along the y axis in the PDB file, the structure was realigned along the z axis to facilitate comparison with the other structures. By assuming that bR is a cylindrical bundle, the tilt (τ) and rotational pitch (ρ) angles were varied between 0–90° and 0–360°, respectively, for simulation of spectra for comparison with the experimental spectrum.

The simulations took into account effects from finite rf pulses as well as imperfect alignment of the membranes by a Gaussian 5° mosaic spread. From a large series of simulations with varying mosaic spread, we determined that even variations in a few degrees cause large changes in the spectra. A 5° mosaic spread gave the best fit with substantial additional line-broadening.

3. Results

3.1. Solid-state NMR measurements

Fig. 1A shows a ^{15}N CP spectrum of [^{15}N]Met-bR in PM oriented with the membrane normal parallel to the external magnetic field (B_0). Two relatively broad signal envelopes are observed in the regions of 150–260 and 30–70 ppm. The former signals, being close to δ_{zz} for an amide site (Cross and Opella, 1994; Teng and Cross, 1989), are assigned to transmembrane helix residues, while the signals around 50 ppm are assigned to residues in the loops. The two sets of signals were deconvoluted and the ratio of the signals from helices and loops was determined to be 3.3:1. Fig. 1B illustrates a PISEMA spectrum of the same [^{15}N]Met-bR sample. In this spectrum, the relatively broad—but still structured—signal envelope from the helix region revealed ^{1}H–^{15}N dipolar couplings of 7–10 kHz, while the loop residues resulted in ^{1}H–^{15}N dipolar couplings of 3–5 kHz. In the corresponding HETCOR spectrum (Fig. 1C), the signals from helical residues were observed with ^{1}H chemical shifts of 0–6 ppm, while loop resonances were observed at 5–11 ppm.

3.2. Deconvolution of the helix signals

Fig. 2A gives a schematic representation of the primary and secondary structure for bR based on the 1C3W crystal structure (Luecke et al., 1999b) and NMR measurements (Saitô et al., 2002). Inspection of some of the reported crystal structures, which may differ due to various sample preparations, the boundaries between helices and loops defined crystallographically (1C3W, 1KME, and 1FBB) differ although there is good agreement for (rigid) helical backbone residues and they indicate 6–7 Met resonances in the helix regions of bR (Hirai and Subramaniam, 2003). Based on the intensity ratio between the helix and loop regions in the 1D (Mason et al., 2004) and PISEMA spectra (Fig. 1), we assume that the helix region of the PISEMA spectrum contains seven NMR resonances while Met-68 and -163 account for the loop resonances which is consistent with hydropathy and sequence analysis. It is immediately clear, however, that the resonances are significantly broader than typically observed for small membrane-reconstituted peptides (Denny et al., 2001;

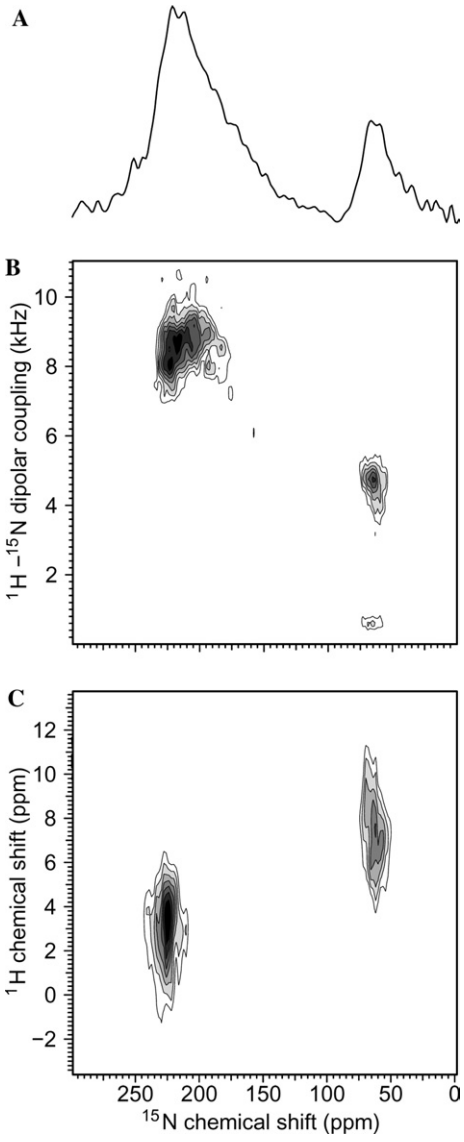

Fig. 1. ^{15}N CP (A), PISEMA (B), and HETCOR (C) flat-coil solid-state NMR spectra of [^{15}N]Met-bR in PM films oriented on glass plates recorded at −20 °C.

Kim et al., 1998; Marassi, 2001; Marassi and Opella, 2000; Marassi et al., 1999, 2000; Nishimura et al., 2002; Ramamoorthy et al., 1999; Song et al., 2000; Wang et al., 2000; Wu et al., 1994). This observation may reflect mosaic spread, local molecular motion (Straus et al., 2003) and may very well be typical for large integral membrane proteins and has a similar analogous description in protein crystallography as the B-factor (Hirai and Subramaniam, 2003). The line-broadening hampers the exact assignment and hence extraction of detailed structural information for every residue. From Fig. 2 it is evident that both the helix and loop signal envelopes are shaped (note in particular the expansion of the helix region in Fig. 2B). These shapes prove to be extremely sensitive to the structure and membrane-embedded conformation of the mole-

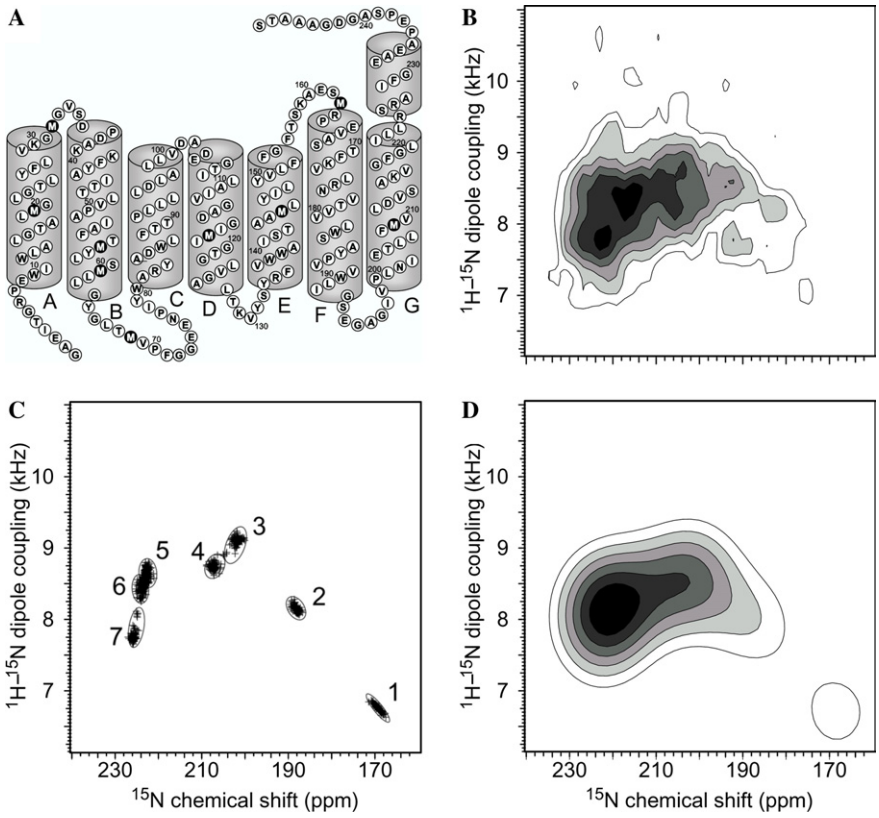

Fig. 2. A schematic representation of the secondary structure of bR based on the 1C3W structure (Luecke et al., 1999b) and NMR measurements (Saitô et al., 2002) highlighting the ^{15}N-labeled Met residues (A). Expansion of the helix region of the PISEMA spectrum in Fig. 1B (B). The 250 best minimizations from multiple fits of simulated to experimental spectra (C). The ellipses define the seven spectral domains denoted 1–7. The simulated spectrum for the helix region based on resonances located in the centers for the seven elliptical regions in (C) with line-widths of 1300 and 800 Hz in the ^{1}H–^{15}N dipolar and ^{15}N chemical shift dimensions, respectively (D).

cule, and thereby a source of important structural information with appropriate interpretation.

To acquire structural information for the helices, the shaped spectral regime from resonances from helix-located ^{15}N residues in the experimental PISEMA spectrum was deconvoluted by fitting it to seven resonances corresponding to Met-20, 32, 56, 60, 118, 145, and 209. Using 16 variables and performing 1000 Monte Carlo-type minimizations starting with random sets of ^{15}N chemical shifts, ^{15}N–^{1}H dipolar couplings, and line-widths, it turned out that 25% of all solutions contained one resonance in each of the seven elliptical domains of resonances illustrated in Fig. 2C. These domains are representative of the seven helix-located Met residues, although they are not assigned in the minimization procedure. Taking the seven centers of the elliptical domains as representative of individual pairs of chemical shift and dipolar coupling parameters, and using the associated line-broadening parameters, the helix region can be represented by the calculated spectrum in Fig. 2D. This spectrum is in very good agreement with the experimental spectrum.

Assuming that the seven methionine resonances originate from seven ideal α-helices with typical torsion angles ($\phi = -65°, \psi = -40°$), it is possible to convert the pairs of ^{15}N chemical shifts and ^{15}N–^{1}H dipolar couplings to restrictions in the helix tilt (τ) and rotational pitch (ρ) angles defined in Fig. 3A. Taking into account some variation in the resonance position this leads to the τ, ρ restriction plots shown in Figs. 3B–D. The restrictions do not take into consideration potential steric hindrance from helix–helix interactions. Based on this analysis, Met-56 and Met-60 can be assigned to the resonances 5, 6 or 6, 7 (or vice versa) since these two residues: (i) belong to the same helix, B, and should have the same tilt angle assuming that there are no helix-breaking residues between them, and (ii) are four residues apart corresponding ideally to a difference of 40° in the rotational pitch. These constraints are compatible with either the 5, 6 (at a tilt of $\tau = 1$–$2°$) or the 6, 7 (at a tilt of $\tau = 5°$) restriction plots. Although it is not possible to make a definitive assignment, it can be concluded that the extracellular half of the helix B in the PM film tilts 1–5° with respect to the bilayer normal. If we apply a similar argument to Met-20 and Met-32 in helix A, ideally with a difference of 120° in the rotational pitch, we find that this may be fulfilled only if these residues are assigned to resonances 7 and 2 or 3, corresponding to a tilt of $\tau = 18$–$22°$. It should be noted that this assignment is less certain than the assignments to helix B since the distance between the two Met residues in helix A is

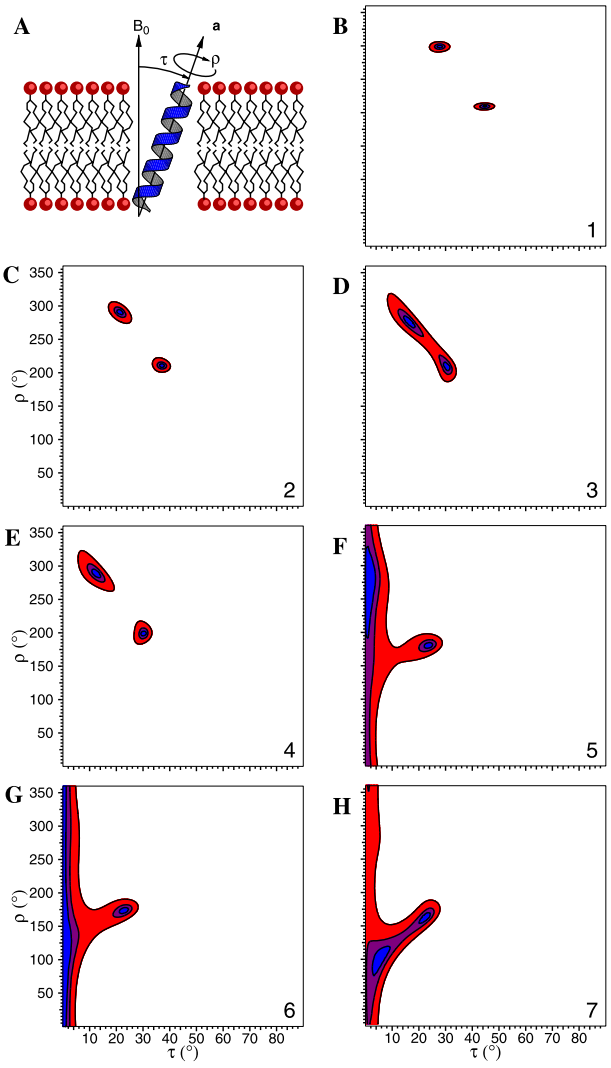

Fig. 3. Definition of the helix tilt (τ) and rotational pitch (ρ) angles for an ideal helix (A). The vector **a** defines the cylindrical axis of the helix. The τ, ρ restriction plots for the seven helix resonances (1–7 as defined in Fig. 2C) (B–H) obtained by attributing the ^{15}N chemical shifts and ^{1}H–^{15}N dipolar couplings in Fig. 2C to the residues in ideal α-helices ($\phi = -65°, \psi = -40°$) and determining for which conformations the resonance frequencies are located within ellipses (blue), 2 (purple), and 4 (red) times the size of the ellipses defining the seven spectral domains (1–7), respectively, in Fig. 2C.

substantially longer than for the two Mets in helix B. The other helices tilt by more than 5°, but cannot be assigned without additional information.

3.3. Comparison with crystal structures

In another approach, the experimental spectra are compared with calculated spectra corresponding to atomic coordinates for some selected crystal structures. This analysis is relevant for two purposes. First, it will reveal the sensitivity of the PISEMA and HETCOR resonance positions towards structural constraints within the accuracy of high-resolution structures. Second, it is

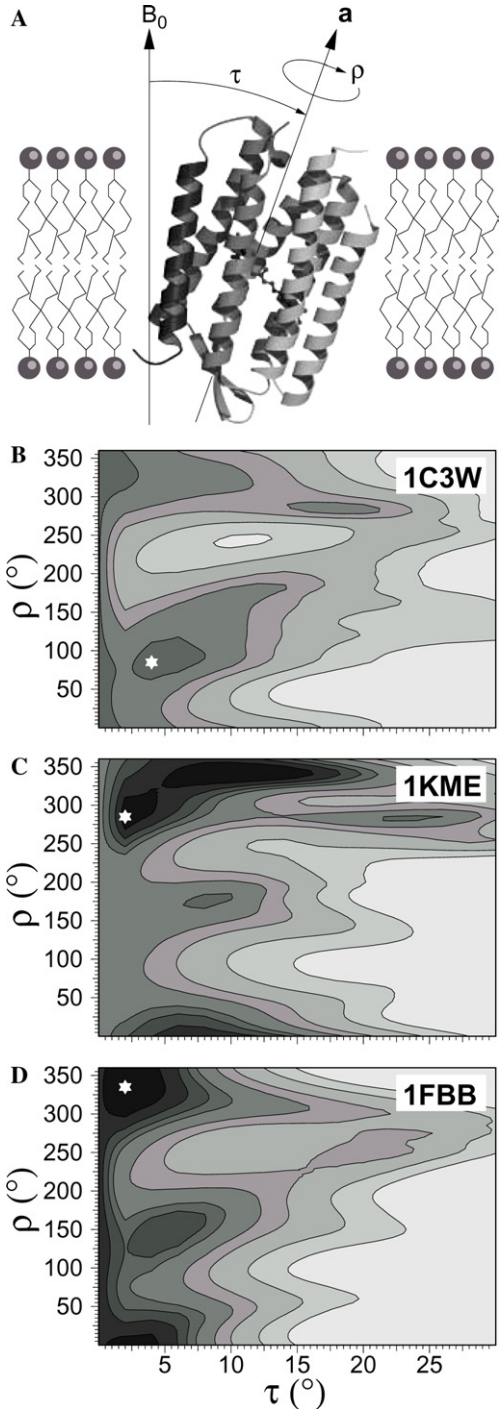

Fig. 4. Definition of the tilt (τ) and rotational pitch (ρ) angle defining the orientation of bR relative to B_0 (A). The vector **a** defines the cylindrical axis of the seven-helix bundle. Contour representation of the RMS deviations between simulated and experimental spectra resulting from a grid scan in τ and ρ for the PISEMA spectra calculated using the atomic coordinates of crystal structures of 1C3W (B), 1KME (C), and 1FBB (D) assuming a 5° mosaic spread. Darker areas correspond to lower RMS values; the position of the minimum RMS values is highlighted by white asterisks. The lowest (τ, ρ) RMS deviations were (4°, 85°) 485, (2°, 285°) 428, and (2°, 335°) 421 for 1C3W, 1KME, and 1FBB, respectively.

possible to examine the compatibility between the structural constraints from solid-state NMR of bR in PM films with the conformation of bR in differently prepared crystalline phases. Specifically, we present results from PDB access codes of 1C3W (3D crystal in lipidic cubic phase, Luecke et al., 1999b), 1KME (3D crystal grown from unique bicelles, Faham and Bowie, 2002), and 1FBB (2D crystal, Subramaniam and Henderson, 2000) and optimized their compatibility with the solid-state NMR spectrum by changing the τ and ρ angles of the overall structure (Fig. 4A). Grid scans showing the RMS deviations between the experimental and simulated PISEMA spectra for the three structures are shown in Figs. 4B–D. The lowest deviations for the τ and ρ angles were obtained at (4°, 85°), (2°, 285°), and (2°, 335°) for 1C3W, 1KME, and 1FBB structures, respectively. The corresponding RMS deviations among the helix signals were 485, 428, and 421. For visual comparison, Figs. 5B–D show the associated simulated PISEMA spectra which can be compared directly with the experimental spectrum (Fig. 5A). Likewise, Figs. 5E–H show the experimental and simulated HETCOR spectra corresponding to the τ, ρ minima in Figs. 4B–D for the three crystal structures.

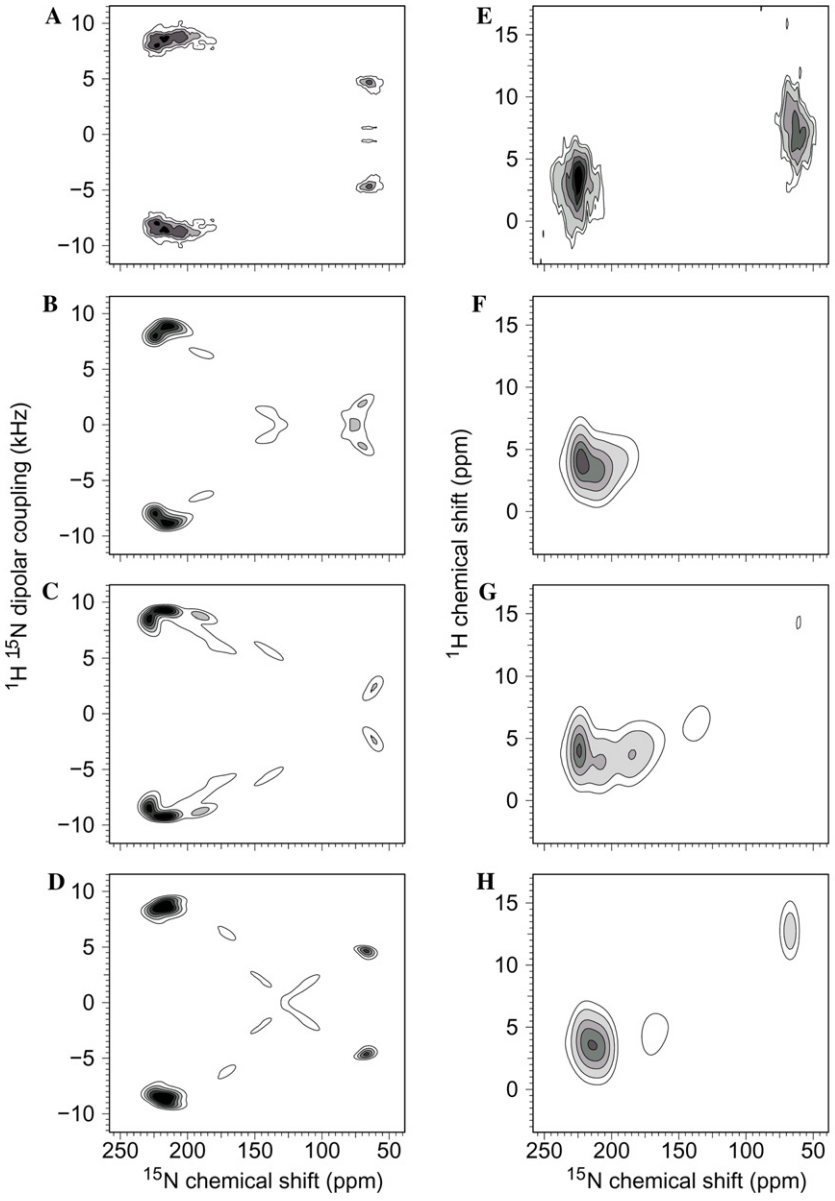

Fig. 5. Experimental (A,E) and simulated PISEMA (B–D) and HETCOR (F–H) spectra corresponding to the RMS minima determined by numerical comparison of experimental and simulated PISEMA spectra in Fig. 4. The spectra correspond to the PDB coordinates and used the same τ, ρ and RMS deviations as those obtained in Fig. 4. All spectra were calculated assuming a 5° mosaic spread.

4. Discussion

Our results demonstrate that important structural and orientational constraints for specifically labeled residues of bR in oriented PM can be established from PISEMA and HETCOR NMR spectra. This applies even though the experimental spectra display relatively low resolution with too broad resonances to allow specific assignment of each residue as previously achieved for well-resolved spectra from single-transmembrane α-helix peptides (Kim et al., 1998; Marassi et al., 1999; Marassi and Opella, 2000; Song et al., 2000; Wang et al., 2000). The lower resolution may be due to the presence of spatial distributions in the sample, mosaic spread, and motion which may be the typical case for large membrane proteins (Straus et al., 2003). Confronted with these facts it is clear that efforts to optimize sample orientation may yield better resolved spectra, but nonetheless, as demonstrated here, the procedures required to extract as much information from less well-resolved spectra as possible are established here. In particular, to compare our experimental PISEMA spectra with simulated spectra corresponding to crystal structures, we consider broadening effects from disorder, mosaic spread, and motion. Not only loops but also helices of bR might have some mobility with small angular amplitudes in the PM film (Straus et al., 2003; Tobian et al., 1995). To a reasonable approximation the anisotropic line-broadening may be masked using a simple Gaussian orientation distribution function in our deconvolution of the experimental spectra. In this manner the line-broadening in the chemical shift and dipolar coupling directions are directly associated with the orientation of the individual peptide planes. Even in presence of a 5° Gaussian mosaic spread, the ^{15}N chemical shifts and ^{15}N–^{1}H dipolar couplings reflect, in a very sensitive manner, the tilt and rotation angles of the peptide planes and thereby the conformation of secondary structure elements in the molecule. Specifically, the conformation of the extracellular side around Met-56 and Met-60 in helix B and a tilt of helix A may be estimated without recourse to any other data.

By deconvolution of the helix region of the PISEMA spectrum, we deduce that the extracellular part of helix B tilts by 1–5° relative to the PM normal by assuming a rotational pitch difference of 40° between Met-56 and Met-60. Likewise, combining a rotational pitch difference of 120° (between Met-20 and Met-32) with the experimentally established structural constraints, a tilt of helix may be deduced to be 18–22°. Although established by simple means, there is a remarkably good agreement between these conclusions and the available crystal data. For example, the tilt of helix B in the crystal structures 1C3W, 1KME, and 1FFB were 3°, 6°, and 5° for the region of the residues 51–62, while the corresponding rotational pitch differences were 51°, 34°, and 43°. Likewise, the tentative estimation of a tilt angle of 18–22° for helix A is close to the tilt angles of 25°, 25°, and 24° (and corresponding rotational pitch differences 102°, 82°, and 95°) determined from the 1C3W, 1KME, and 1FBB structures (Faham and Bowie, 2002; Luecke et al., 1999b; Subramaniam and Henderson, 2000). In addition, it can be concluded from the restriction plots that the remaining Met-containing helices (D, E, and G) have tilts larger than 5–8°, being in agreement with the available structures. Thus, ''blind'' deconvolution of the spectra is in close agreement with high-resolution data for crystalline bR, supporting the suggestion that the structure and membrane-associated conformation of helices A and B is closely convergent for different crystal forms (Hirai and Subramaniam, 2003).

In addition to direct structural information, the data here demonstrate for the first time that it is possible to establish a direct comparison of crystal and PM structures for bR which may be of general interest for the application of XRD and solid-state NMR in membrane protein characterization. Our simulations reveal that the PISEMA and HETCOR spectra are extremely sensitive to the local conformation of the protein. Although it was reported that the RMS deviation between the bR monomers of 1C3W and 1KME is only 0.72 Å (Faham and Bowie, 2002), the PISEMA spectra simulated from the atomic coordinates are widely different due to sensitivity of the ^{15}N–^{1}H dipolar couplings toward changes in the orientation of the peptide plane relative to B_0. The experimental data from PM film which preserves the 2D crystalline lattice (Fitter et al., 1999; Seiff et al., 1985) are closer to the spectra obtained from 1FBB and 1KME structures rather than 1C3W. However, the PISEMA and HETCOR spectra resulting from 1KME (Figs. 5C and G) and 1FBB (Figs. 5D and H) are slightly different from the experimentally obtained spectrum (Figs. 5A and E), suggesting that some differences exist between the protein conformation in the sample used here when compared with crystal forms. This may be attributed to differences in sample preparation, temperature, and most interestingly, the protein packing.

In conclusion, we have demonstrated that oriented-sample solid-state NMR spectroscopy is feasible for the study of large integral membrane proteins. This is a first step for a structural determination of a seven-transmembrane protein embedded in its natural environment using oriented solid-state NMR methods and simulations. With further optimization of the sample alignment procedures and by a combination of results for different residue-specific labeling, the method has the potential for resolving full backbone structures for large integral membrane proteins. Even with a less ambitious view, it is clear that solid-state NMR on specifi-

cally labeled samples may provide valuable information on conformational changes upon activation of membrane proteins. As demonstrated here, this applies even though the sample has relatively large mosaic spread—a situation that may be representative for many large integral membrane proteins amenable to solid-state NMR characterization.

Acknowledgments

This work was supported by the Medical Research Council (UK) and Biotechnology and Biology Research Council with grants to A.W., and Carlsbergfondet, The Danish Biotechnological Instrument Centre (DABIC), Novo Nordisk Fonden, and the Danish Natural Science Research Council with grants to N.C.N. S.K.S. acknowledges support from the Royal Society for a Dorothy Hodgkin Research Fellowship.

References

Bak, M., Rasmussen, J.T., Nielsen, N.C., 2000. SIMPSON: a general simulation program for solid-state NMR spectroscopy. J. Magn. Reson. 147, 296–330.

Bak, M., Schultz, R., Vosegaard, T., Nielsen, N.C., 2002. Specification and visualization of anisotropic interaction tensors in polypeptides and numerical simulations in biological solid-state NMR. J. Magn. Reson. 154, 28–45.

Bielecki, A., Kolbert, A.C., De Groot, H.J.M., Griffin, R.G., Levitt, M.H., 1990. Frequency-switched Lee–Goldburg sequences in solids. Adv. Magn. Reson. 14, 111–124.

Bjerring, M., Vosegaard, T., Malmendal, A.B., Nielsen, N.C., 2003. Methodological development of solid-state NMR for characterization of membrane proteins. Concepts Magn. Reson. 18A, 111–129.

Cross, T.A., Opella, S.J., 1994. Solid-state NMR structural studies of peptides and proteins in membranes. Curr. Opin. Struct. Biol. 4, 574–581.

Denny, J.K., Wang, J., Cross, T.A., Quine, J.R., 2001. PISEMA powder patterns and PISA wheels. J. Magn. Reson. 152, 217–226.

Edman, K., Nollert, P., Royant, A., Belrhali, H., Pebay-Peyroula, E., Hajdu, J., Neutze, R., Landau, E.M., 1999. High-resolution X-ray structure of an early intermediate in the bacteriorhodopsin photocycle. Nature 401, 822–826.

Faham, S., Bowie, J.U., 2002. Bicelle crystallization: a new method for crystallizing membrane proteins yields a monomeric bacteriorhodopsin structure. J. Mol. Biol. 316, 1–6.

Fitter, J., Lechner, R.E., Dencher, N.A., 1999. Interactions of hydration water and biological membranes studied by neutron scattering. J. Phys. Chem. B 103, 8036–8050.

Helgerson, S.L., Siemsen, S.L., Dratz, E.A., 1992. Enrichment of bacteriorhodopsin with isotopically labeled amino acids by biosynthetic incorporation in *Halobacterium halobium*. Can. J. Microbiol. 38, 1181–1185.

Herzfeld, J., Lansing, J.C., 2002. Magnetic resonance studies of the bacteriorhodopsin pump cycle. Annu. Rev. Biophys. Biomol. Struct. 31, 73–95.

Hirai, T., Subramaniam, S., 2003. Structural insights into the mechanism of proton pumping by bacteriorhodopsin. FEBS Lett. 545, 2–8.

Kim, Y., Valentine, K., Opella, S.J., Schendel, S.L., Cramer, W.A., 1998. Solid-state NMR studies of the membrane-bound closed state of the colicin E1 channel domain in lipid bilayers. Protein Sci. 7, 342–348.

Lanyi, J.K., 1993. Proton translocation mechanism and energetics in the light-driven pump bacteriorhodopsin. Biochim. Biophys. Acta 1460, 133–156.

Lanyi, J.K., 1997. Mechanism of ion transport across membrane. Bacteriorhodopsin as a prototype for proton pump. J. Biol. Chem. 272, 31209–31212.

Lanyi, J., Schobert, B., 2002. Crystallographic structure of the retinal and the protein after deprotonation of the Schiff base: the switch in the bacteriorhodopsin photocycle. J. Mol. Biol. 321, 727–737.

Lee, M., Goldburg, W., 1965. Nuclear-magnetic-resonance line narrowing by a rotating rf field. Phys. Rev. 140, 1261–1271.

Levitt, M.H., 1991. Heteronuclear cross polarization in liquid-state nuclear magnetic resonance: mismatch compensation and relaxation behavior. J. Chem. Phys. 94, 30–38.

Luecke, H., Schobert, B., Richter, H.T., Cartailler, J.P., Lanyi, J.K., 1999a. Structural changes in bacteriorhodopsin during ion transport at 2 Å resolution. Science 286, 255–260.

Luecke, H., Schobert, B., Richter, H.T., Cartailler, J.P., Lanyi, J.K., 1999b. Structure of bacteriorhodopsin at 1.55 Å resolution. J. Mol. Biol. 291, 899–911.

Marassi, F.M., 2001. A simple approach to membrane protein secondary structure and topology based on NMR spectroscopy. Biophys. J. 80, 994–1003.

Marassi, F.M., Opella, S.J., 2000. A solid-state NMR index of helical membrane protein structure and topology. J. Magn. Res. 144, 150–155.

Marassi, F.M., Gesell, J.J., Valente, A.P., Kim, Y., Oblatt-Montal, M., Montal, M., Opella, S.J., 1999. Dilute spin-exchange assignment of solid-state NMR spectra of oriented proteins: acetylcholine M2 in bilayers. J. Biomol. NMR 14, 141–148.

Marassi, F.M., Ma, C., Gesell, J.J., Opella, S.J., 2000. Three-dimensional solid-state NMR spectroscopy is essential for resolution of resonances from in-plane residues in uniformly (15)N-labeled helical membrane proteins in oriented lipid bilayers. J. Magn. Reson. 144, 156–161.

Mason, A.J., Grage, S.L., Straus, S.K., Clemens, G., Watts, A., 2004. Identifying anisotropic constraints in multiply labelled bacteriorhodopsin by ^{15}N MAOSS NMR: a general approach to structural studied of membrane proteins. Biophys. J. 86, 1610–1617.

Mathies, R.A., Lin, S.W., Ames, J.B., Pollard, W.T., 1991. From femtoseconds to biology: mechanism of bacteriorhodopsin's light-driven proton pump. Annu. Rev. Biophys. Chem. 20, 491–518.

Nishimura, K., Kim, S., Zhang, L., Cross, T.A., 2002. The closed state of a H^+ channel helical bundle combining precise orientational and distance restraints from solid state NMR. Biochemistry 41, 13170–13177.

Oesterhelt, D., Stoeckenius, W., 1974. Isolation of the cell membrane of *Halobacterium halobium* and its fractionation into red and purple membrane. Methods Enzymol. 31, 667–678.

Oesterhelt, D., Brauchle, C., Hampp, N., 1991. Bacteriorhodopsin: a biological material for information processing. Q. Rev. Biophys. 24, 425–478.

Ovchinnikov, Y., 1982. Rhodopsin and bacteriorhodopsin: structure–function relationships. FEBS Lett. 148, 179–191.

Papadopoulos, G., Dencher, N.A., Zaccai, G., Büldt, G., 1990. Water molecules and exchangeable hydrogen ions at the active centre of bacteriorhodopsin localized by neutron diffraction. Elements of the proton pathway?. J. Mol. Biol. 214, 15–19.

Ramamoorthy, A., Wu, C.H., Opella, S.J., 1999. Experimental aspects of multidimensional solid-state NMR correlation spectroscopy. J. Magn. Reson. 140, 131–140.

Royant, A., Edman, K., Ursby, T., Pebay-Peyroula, E., Landau, E.M., Neutze, R., 2001. Spectroscopic characterization of bacteriorho-

dopsin's L-intermediate in 3D crystals cooled to 170 K. Photochem. Photobiol. 74, 794–804.

Saitô, H., Tuzi, S., Naito, A., 1998. Empirical vs. nonempirical evaluation of secondary structure of fibrious and membrane proteins. Annu. Rep. NMR Spectrosc. 36, 79–121.

Saitô, H., Tuzi, S., Yamaguchi, S., Tanio, M., Naito, A., 2000. Conformation and backbone dynamics of bacteriorhodopsin revealed by ^{13}C-NMR. Biochim. Biophys. Acta 1460, 39–48.

Saitô, H., Tuzi, S., Tanio, M., Naito, A., 2002. Dynamic aspect of membrane proteins and membrane associated peptides as revealed by ^{13}C NMR: lessons from bacteriorhodopsin as an Intact protein. Annu. Rep. NMR Spectrosc. 47, 39–108.

Sass, H., Büldt, G., Gessenich, R., Hehn, D., Neff, D., Schlesinger, J., Berendzen, J., Ormos, P., 2000. Structural alterations for proton translocation in the M state of wild-type bacteriorhodopsin. Nature 40, 649–653.

Schobert, B., Cupp-Vickery, J., Hornak, V., Smith, S., Lanyi, J., 2002. Crystallographic structure of the K intermediate of bacteriorhodopsin: conservation of free energy after photoisomerization of the retinal. J. Mol. Biol. 321, 715–726.

Seiff, F., Wallat, I., Ermann, P., Heyn, M.P., 1985. A neutron diffraction study on the location of the polyene chain of retinal in bacteriorhodopsin. Proc. Natl. Acad. Sci. USA 82, 3227–3231.

Song, Z., Kovacs, F.A., Wang, J., Denny, J.K., Shekar, S.C., Quine, J.R., Cross, T.A., 2000. Transmembrane domain of M2 protein from influenza A virus studied by solid-state (15)N polarization inversion spin exchange at magic angle NMR. Biophys. J. 79, 767–775.

Stoeckenius, W., Bogomolni, R.A., 1982. Bacteriorhodopsin and related pigments of Halobacteria. Annu. Rev. Biochem. 1982, 587–616.

Straus, S.K., Scott, W., Watts, A., 2003. Assessing the effects of time and spatial averaging in ^{15}N chemical shift/^{15}N–^{1}H dipolar correlation solid state NMR experiments. J. Biomol. NMR 26, 283–295.

Subramaniam, S., Henderson, R., 2000. Molecular mechanism of vectorial proton translocation by bacteriorhodopsin. Nature 406, 653–657.

Teng, G., Cross, T.A., 1989. Tensor orientation in a polypeptide. J. Magn. Reson. 85, 439–447.

Tobian, D.J., Gesell, J., Klein, L., Opella, S.J., 1995. A simple protocol for identification of helical and mobile residues in membrane proteins. J. Mol. Biol. 253, 391–395.

Ulrich, A.S., Heyn, M.P., Watts, A., 1992. Structure determination of the cyclohexene ring of retinal in bacteriorhodopsin by solid-state deuterium NMR. Biochemistry 31, 10390–10399.

Ulrich, A.S., Watts, A., Wallat, I., Heyn, M.P., 1994. Distorted structure of the retinal chromophore in bacteriorhodopsin resolved by ^{2}H-NMR. Biochemistry 33, 5370–5375.

Ulrich, A.S., Wallat, I., Heyn, M.P., Watts, A., 1995. Re-orientation of retinal in the M-photointermediate of bacteriorhodopsin. Nat. Struct. Biol. 2, 190–192.

Vosegaard, T., Nielsen, N.C., 2002. Towards high-resolution solid-state NMR on large uniformly ^{15}N- and [^{13}C,^{15}N]-labeled membrane proteins in oriented lipid bilayers. J. Biomol. NMR 22, 225–247.

Vosegaard, T., Malmendal, A., Nielsen, N.C., 2002. The flexibility of SIMPSON and SIMMOL for numerical simulations in solid- and liquid-state NMR spectroscopy. Chem. Monthly 133, 1555–1574.

Wang, J., Denny, J.K., Tian, C., Kim, S., Mo, Y., Kovacs, F.A., Song, Z., Nishimura, K., Gan, Z., Fu, R., Quine, J.R., Cross, T.A., 2000. Imaging membrane protein helical wheels. J. Magn. Reson. 144, 162–167.

Wu, C.H., Ramamoorthy, A., Opella, S.J., 1994. High resolution heteronuclear dipolar solid-state NMR spectroscopy. J. Magn. Reson. A 109, 270–272.